OPEN ACCESS
IOP Publishing
Smart Materials and Structures
Smart Mater. Struct. **33** (2024) 105047 (15pp)
https://doi.org/10.1088/1361-665X/ad7d56

# *In situ* assembly enabling adhesive-free bonding of large area electronic sensors to concrete for structural health monitoring

**Emmanuel Ogunniyi[1], Han Liu[2], Austin RJ Downey[1,3,*], Simon Laflamme[2,4], Jian Li[5], Caroline Bennett[5], William Collins[5], Hongki Jo[6] and Paul Ziehl[1,3]**

[1] Department of Mechanical Engineering, University of South Carolina, Columbia, SC, United States of America
[2] Department of Civil, Construction, and Environmental Engineering, Iowa State University, Ames, IA, United States of America
[3] Department of Civil and Environmental Engineering, University of South Carolina, Columbia, SC, United States of America
[4] Department of Electrical and Computer Engineering, Iowa State University, Ames, IA, United States of America
[5] Department of Civil, Environmental and Architectural Engineering, The University of Kansas, Lawrence, KS, United States of America
[6] Department of Civil, Architectural Engineering and Mechanics, The University of Arizona, Tucson, AZ, United States of America

E-mail: austindowney@sc.edu

Received 18 June 2024, revised 4 September 2024
Accepted for publication 19 September 2024
Published 1 October 2024


**Abstract**

Cracks developed in concrete infrastructure are one of the primary mechanisms that degrade their structural integrity, which may result in structural failures. Previous research on soft elastomeric capacitors (SEC) has shown their viability for structural health monitoring of structural materials, including concrete, steel, and fiberglass composites. The SEC, or its derivative version with a corrugated geometry termed corrugated SEC or cSEC, is a parallel plate capacitor. Prior work demonstrated that it was possible to directly paint the electrode interfacing with the structural material onto the structure and adhere the rest of the pre-fabricated sensor onto the wet interface, thereby eliminating the need for a joining epoxy. This demonstration was conducted on steel and fiberglass. The study on concrete was left to future work as concrete exhibits a much rougher surface and structure/sensor capacitive coupling, causing a significant amplification in signal noise. This study advances structural health monitoring in concrete applications by investigating the *in situ* assembly of the SEC on concrete where the carbon black (CB)-based electrode plate of the cSEC is directly painted onto the concrete surface and serves as both the adhesive and electrode for the sensor. A series of

* Author to whom any correspondence should be addressed.

free-vibration and compression tests were designed and conducted to evaluate the sensing performance of *in situ* assembled cSEC compared to that of an epoxy-bonded cSEC. Additionally, the bonding strength of the *in situ* assembled and epoxy-bonded cSEC is evaluated through a peel test. Results show good strain sensing capabilities of the *in situ* assembled SEC with an $R^2$ value of 0.986 and a resolution of 45 $\pm\mu\varepsilon$. Even though the epoxied cSEC demonstrated a higher bonding strength than the *in situ* assembled cSEC, the *in situ* assembled cSEC demonstrated adequate bonding strength for the application. This research contributes to the scientific understanding of sensor adhesion and opens avenues for practical applications in infrastructure monitoring, potentially leading to more resilient and sustainable urban environments.

Keywords: soft elastomeric capacitors, sensor adhesion, flexible sensors, concrete strain, structural health monitoring, large-area electronics, sensing skins

## Abbreviations

*The following abbreviations are used in this manuscript:*

| | |
|---|---|
| LAE | Large-area electronics |
| SHM | Structural health monitoring |
| SEBS | Styrene-ethylene-butadiene-Styrene |
| CB | Carbon black |
| cSEC | Corrugated soft elastomeric capacitor |
| ST | Strain transducer |
| RSG | Resistive strain gauge |

## 1. Introduction

Structural health monitoring (SHM) involves the automatic assessment of a structure's integrity and health condition, encompassing an impressive integration of engineering practices, technological advancements, and safety protocols [1, 2]. A crucial aspect of SHM is its dependence on sophisticated sensor technologies, ranging from accelerometers, strain gauges, and acoustic sensors to optical fibers [3, 4].

SHM of concrete structures is advancing through the integration of diverse sensing technologies that cater to various monitoring needs, both internal [5] and surface [6]. This dual approach is crucial for a comprehensive assessment of structural health [7]. Surface strain monitoring is essential for detecting visible deformations, while internal strain monitoring plays a critical role in identifying early-stage cracks that often originate within of the concrete structure. Fiber optic sensors, including Fiber bragg gratings and distributed sensing methods like Rayleigh and Brillouin scattering, are primarily used for internal strain monitoring due to their high sensitivity [8] and real-time ability [9] to monitor strain over large areas, despite their expense, fragility, and complex installation procedures [10]. Piezoelectric sensors are versatile, employed for both internal and surface strain monitoring, especially for detecting dynamic strain and vibrations [11]. Traditional methods, such as electrical resistance strain gauges [12] and vibrating wire strain gauges [13], are typically used for surface strain monitoring, valued for their simplicity but limited by their sensitivity and durability.

Advancements in concrete structural monitoring are furthered by wireless sensor networks and internet of things (IoT) technologies, which enable remote, real-time data collection and analysis [14, 15]. Distributed acoustic sensing is employed for continuous internal strain monitoring over large structures [16], while Acoustic emission sensors and ultrasonic testing methods are critical for the early detection of internal flaws [17]. Non-contact methods like Laser Doppler Vibrometry [18] and thermographic cameras [19] are used for surface strain and thermal stress monitoring, offering innovative approaches to SHM of concrete structures. These technologies facilitate detailed tracking of a structure's integrity by continuously recording data on vital physical parameters, including vibration, temperature, displacement, and strain. This continuous data stream enables real-time diagnostics and prognostics of structural states, which are crucial for the prompt execution of maintenance, necessary repairs, and the replacement of components, thereby ensuring the longevity and safety of the structure.

The deployment of these SHM technologies in the field has been traditionally hindered by cost, complex installation processes, especially on intricate geometries, and the relatively small size of commercially available sensing technologies, making it difficult to detect, localize, quantify, and predict damages across extensive areas. However, the remarkable efficiencies and attributes of natural and biological systems have paved the way for the development of bio-inspired sensors, as highlighted in the work by Jung *et al* [20] and Masciotta *et al* [21]. A prime example of such innovation is sensing skin technology, a form of large-area electronics (LAE) capable of transducing local deformations into a measurable state. This technology enables the creation of a densely packed sensor network, which can be strategically deployed at various locations of a structure. This approach yields high-resolution data, providing a more thorough and nuanced understanding of structural health than what is achievable through traditional methods.

Large-area electronics technology have been previously introduced by developing a soft elastomeric capacitor (SEC). The SEC, constructed using a layer-by-layer technique with a styrene-ethylene-butylene-styrene (SEBS) block copolymer matrix, creates a sensor with notable flexibility, ductility, and

compliance [22]. The operational principle of SECs is founded on the variation in capacitance caused by mechanical strains or deformations exerted on the elastomeric material. When external forces are applied, they alter the geometry of the dielectric, leading to a measurable change in the sensor's capacitance where changes in capacitance are directly related to the physical deformation of the sensor. The capacitance measurements obtained from the SEC can be translated into various structural parameters, such as strain, stress, fatigue cracks, humidity, impact energy, etc. This translation is possible through the electromechanical model that defines the relationship between capacitance and the specific parameter of interest [23, 24]. The SEC has proven to be extremely valuable in monitoring the health of bridges [25], detecting and tracking fatigue cracks [26] offering advantages such as less expensive to fabricate, customizable shapes and sizes to cover large areas, long term durability and weatherability, can be used on irregular geometries because of their flexibilities and low energy requirements. Prior research demonstrated that the SEC maintains its functionality and signal integrity over extended periods under a range of environmental conditions, including simulated thermal, high humidity, and exposure to UV radiation cycles [27].

In the study by Liu *et al* [26], the performance of the corrugated SEC (cSEC) was evaluated without bonding to any substrate. The results demonstrated that the SEC exhibits excellent linearity and sensitivity, with the gauge factor increased by approximately 30% and signal accuracy improved by 35% with added corrugations. The SEC maintained remarkable stability and accuracy under varying strain levels and loading conditions, establishing a solid baseline for its performance independently of substrate effects. The study highlighted the SEC's ability to provide precise and repeatable strain measurements, essential for applications in SHM. The SEC is built with materials resistant to moisture, UV degradation, and environmental stressors. Titania inclusions enhance the dielectric's weather durability, while carbon black (CB) doped conductive layers offer high durability and weather protection. To mitigate capacitive coupling between the electrode and concrete [28], an additional SEBS polymer layer was added on the top of the conductive layer [29], resulting in an electrically isolated SEC.

Similar or comparable large-area capacitive sensor technologies have shown usefulness in on-human applications. Devaraj *et al* assembled a highly elastic and flexible capacitive pressure/force sensing array from elastic conductive thin films of CB composite to be used as a capacitive sensor array for soft robotics [30]. In a similar thrust, Atalay developed a textile-based strain sensor for wearable applications [31]. These endeavors showcase its broad potential and significant impact across various domains.

The effectiveness and reliability of SECs (and cSECs) are significantly influenced by the quality of their adhesion to the substrates they monitor. Optimal sensor performance, durability, and longevity hinge on this adhesion. Poor bonding is known to lead to delamination, decreased sensitivity, and loss of electrical contact, which can severely impair the sensor's functionality and service life. Yet, adhesive application, for instance using a bi-component epoxy, can be time consuming [32], and the bond strength needs to be considered especially when deploying several sensors onto a substrate [33]. As a solution, the authors developed a paintable version of the cSEC. Instead of SEBS, the paintable cSEC's matrix is based on silicone to achieve reliable sensor bonding without necessitating an epoxy [34]. Introductory work on the paintable cSEC was conducted on steel and fiberglass. The study on concrete was left to future work because concrete exhibits a much rougher surface and structure/sensor capacitive coupling causing a significant amplification in signal noise.

This study extends work on the *in situ* assembled cSEC by investigating its application to concrete. Inspired from prior work, the method involves directly adhering the cSEC to the target surface using a CB solution as the bonding agent which also concurrently serves as the sensor electrode, offering a straightforward alternative to traditional bonding techniques. Unlike prior work, the pre-fabricated portion of the cSEC is SEBS-based instead of silicone-based, because work in [28] has shown the promise of the SEBS-based SECs in concrete applications. Further comparisons were made between this approach and the traditional epoxy bonding technique. The *in situ* assembled cSEC performance is initially assessed through a series of tests to understand its sensing capabilities. These evaluations include quasi-static and free vibration tests performed on an aluminum cantilever plate designed to characterize the sensor's response under homogeneous and controlled conditions. The study further investigates the sensor's performance by applying cyclic compression loading tests to concrete samples. During these tests, *in situ* assembled and epoxied cSECs are utilized to measure the strain responses, with measurements benchmarked against a reference strain transducer acting as ground truth. Additionally, a peel test designed following ASTM D903 at 180 degree peel angle was executed to evaluate the adhesion strength of the two bonding methods [35]. The contributions of this work are threefold, (1) introduces the use of a CB solution as both the electrode and bonding agent for *in situ* assembled cSEC on concrete surfaces, simplifying sensor installation by eliminating the need for external epoxy. (2) Conducting comparative analyses between the new CB solution bonding method and the traditional epoxy bonding technique to assess performance differences. (3) Executing a peel test according to ASTM D903 standards to evaluate the adhesion strength of the CB solution bonding method compared to the traditional epoxy method.

## 2. Background

This section provides a necessary background of the cSEC, which includes the fabrication process of the dielectric layer and the electromechanical model.

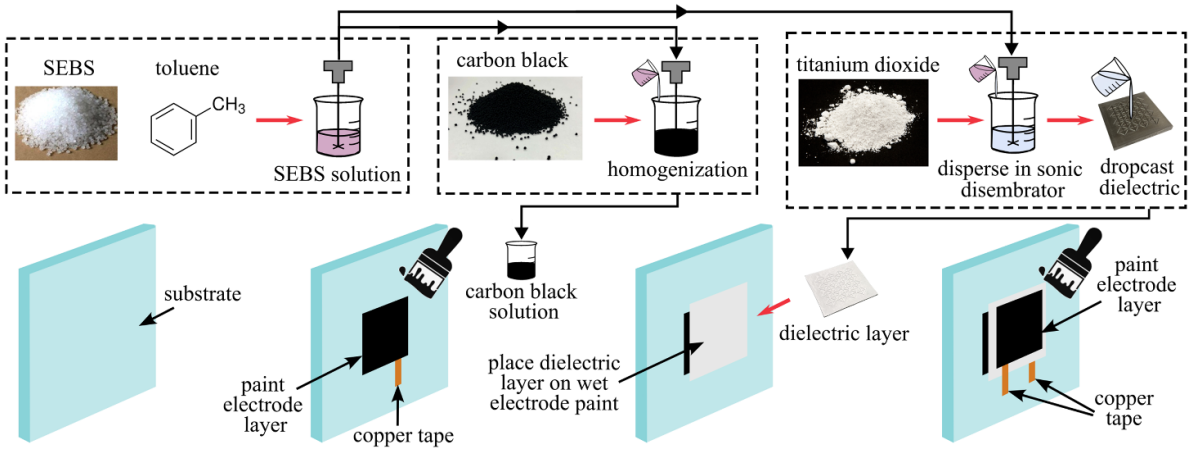


**Figure 1.** Fabrication process of the *in situ* assembly of the corrugated SEC (cSEC).

### *2.1. SEC sensor manufacturing*

A cSEC is a highly compliant thin-film strain sensor consisting of a dielectric layer between two conductive layers, constituting a parallel plate capacitor. The methodology for fabricating the cSEC is as depicted in figure 1. The corrugated structure of the dielectric layer is achieved through a precise drop-casting process, which is elaborated on in the subsequent sections.

i. SEBS FG1901G (KRATON, USA, $\rho = 1400$ kg m$^{-3}$ 30%w styrene) and SEBS 50 0120 M (VTC Elastoteknik AB, Sweden, $\rho = 930$ kg m$^{-3}$) were mixed with a weight ratio of 1:3 and dissolved in a reagent grade toluene at a concentration of 160 g l$^{-1}$. PDMS-coated titania $TiO_2(OSI(CH_3)^{2-})$ (TPL, Inc. Albuquerque, NM) particles with an average diameter of 100 nm is added in 3 wt% to 20 ml of the prepared SEBS/toluene solution at a concentration of 75 g l$^{-1}$.
ii. Rutile titania particles are uniformly dispersed in the SEBS matrix using a sonic dismembrator (high-intensity ultrasonic processor Vibracell 75 041, Sonics & Materials Inc. USA) for five minutes at 20 kHz and 120 Watt, and the SEBS-titania solution sits in an iced water bath for cooling.
iii. The resulting SEBS-titania solution is drop-cast directly onto an 80 × 80 mm non-stick square steel mold (H13 steel with HRC48-50 hardness), designed with grooves for creating surface corrugation. The drop-casted solution is covered to control evaporation under room temperature and left in a fume hood to dry over 24 h.
iv. The film is peeled from the mold after drying, and quality is controlled by measuring the thickness, in which the resulting film has a mean thickness of 0.4 mm over the non-corrugated area and a corrugation height of 0.35 mm. The resulting dielectric layer is shown in figure 2(a). Any dielectric specimen with a thickness variation of more than 0.05 mm on the measured area is identified as non-conforming and was discarded and re-fabricated.

The electrodes are made of the same organic matrix as the dielectric layer to have robust mechanical interlayer bonding, but were doped with CB particles to provide the sensor with the required conductivity and environmental robustness. The fabrication of the electrodes (CB solution) is described below.

i. SEBS 50 0050 M (VTC Elastoteknik AB, Sweden) is dissolved in toluene at a concentration of 380 g l$^{-1}$, and CB particles (ORION, Kingwood, TX) are added in 2.75 wt% to 15 ml of the prepared SEBS/toluene solution at a concentration of 25 g l$^{-1}$. The added CB particles are uniformly dispersed using a low-speed homogenizer for one hour at 650–850 rpm.
ii. The resulting SEBS-CB solution is brushed onto the dielectric layer's top and bottom surfaces as electrodes. Four conductive layers are brushed on, with a 5 min drying time between each layer, followed by an additional 24 h drying time after four iterations of brushing.
iii. Two adhesive copper tapes are glued on both sides of the composite film to serve as the electrical connections for the data acquisition system (DAQ), and a thin layer of the PELCO conductive carbon glue (TED Pella, USA) is applied to coat the exposed parts of copper tapes over the electrodes, enhancing bonding strength and minimizing added noise.

The resulting cSEC used has an initial capacitance between 220 and 260 pF under a 1 kHz measuring frequency. Figure 2(c) shows a picture of a cSEC unit, corrugated with a patterned termed reinforced diagrid.

### *2.2. Electromechanical model*

At low sampling rates (<1 kHz), the cSEC can be modeled as a non-lossy parallel plate capacitor, and an electro-mechanical model that relates a change in area of the monitored structure to a measurable change in capacitance can be derived by taking the initial capacitance ($C_0$):

$$C_0 = e_0 e_r \frac{A}{h} \tag{1}$$

where $e_0 = 8.854$ pF m$^{-1}$ is the vacuum permittivity, $e_r$ is the relative permittivity of the polymer, $A = l \times w$ is the electrode

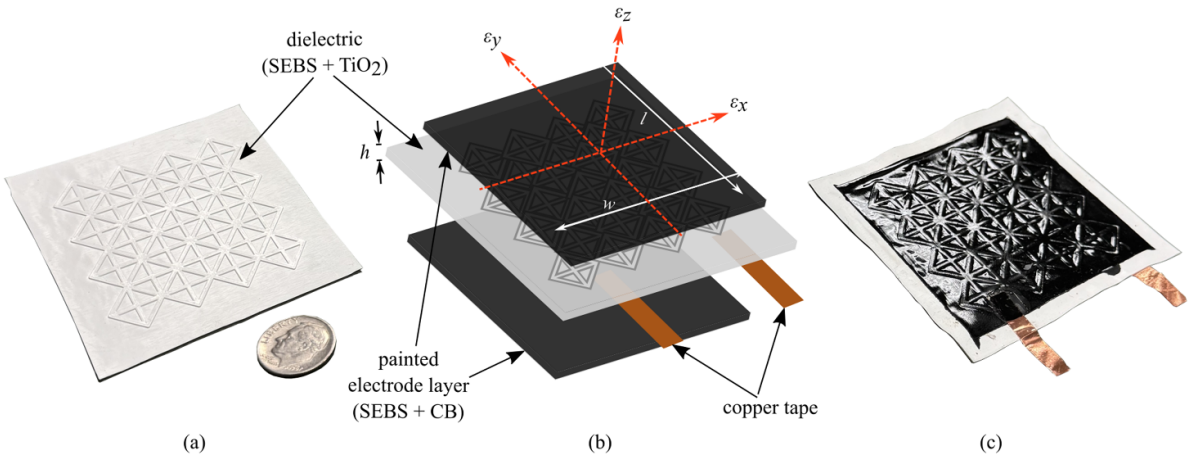


**Figure 2.** A soft elastomeric capacitor where (a) is dielectric layer with a reinforced diagrid pattern; (b) schematic showing the parallel plate capacitor structure of the cSEC with key components and reference axes annotated; and (c) a 76 × 76 mm ($l \times w$) cSEC.

area of length $l$ and width $w$, and $h$ indicates the thickness of the dielectric (as annotated in figure 2(b)). By differentiating equation (1), the relative change in capacitance ($\Delta C/C_0$) under a small strain along the $x$-direction can be obtained:

$$\frac{\Delta C}{C_0} = \left(\frac{\Delta l}{l_0} + \frac{\Delta w}{w_0} + \frac{\Delta h}{h_0}\right) = \varepsilon_x + \varepsilon_y - \varepsilon_z \tag{2}$$

where $\Delta$ denotes a change in the variable due to strain. Apply Hooke's Law under the assumption of plane stress, one obtains:

$$\frac{\Delta C}{C_0} = \frac{1}{1-\nu_0}\left(\varepsilon_x + \varepsilon_y\right) = \lambda_0\left(\varepsilon_x + \varepsilon_y\right). \tag{3}$$

The presence of surface corrugation on the dielectric layer results in an orthotropic composite, altering the Poisson's ratio in the $x-y$ plane, denoted as $\nu_{xy} = -\frac{-\varepsilon_y}{\varepsilon_x}$. Consequently, equation (3) can be rewritten as follows:

$$\frac{\Delta C}{C_0} = \frac{1-\nu_{xy}}{1-\nu}\varepsilon_x = \lambda\varepsilon_x. \tag{4}$$

When the sensor is adhered, the transverse Poisson's ratio is altered due to the composite effect with the materials to which the sensor is adhered, and the composite transverse Poisson's ratio $\nu_{xy,c}$ can be expressed as:

$$\nu_{xy,c} = \frac{a\nu_{xy} + b\nu_m}{a+b} \tag{5}$$

where $\nu_m$ is the Poisson's ratio of the monitored material, and $a$ and $b$ are weight coefficients depend on the level of adhesion and material stiffness and constrained by $a+b=1$. Therefore, the resulting gauge factor under the composite effect $\lambda_c$ can be written as:

$$\lambda_c = \frac{1-\nu_{xy,c}}{1-\nu}. \tag{6}$$

## 3. Methodology

This section details the procedure for the *in situ* assembly of the cSEC and the experimental setup to assess the sensor's performance. First, the quasi-static and free vibration tests used to characterize the sensing performance of *in situ* assembled cSEC are described. Second, the experimental procedure compression test conducted on concrete specimens is presented. Third, the peel test design is demonstrated to evaluate the adhesion strength of cSECs.

### 3.1. In situ sensor assembly

The adhesion procedure initiated with the preparation of a clean, smooth area on the concrete surface to ensure optimal sensor attachment. This preparation involved mechanically abrading the concrete with 3 M 314D P180 sandpaper to remove any roughness, providing a uniform surface for the sensor. Dust, dirt, and loose particles were eliminated further by cleaning the area using a combination of compressed air and a brush, effectively preparing the surface for the next step. After this initial cleaning, acetone was employed to remove any traces of oil, grease, or organic contaminants, ensuring the surface was free of substances that could impair adhesion. The final step in the preparation process involved thoroughly rinsing the concrete with water and allowing it to dry completely, creating an ideal surface for the practical attachment of the cSEC.

The direct painting (*in situ* assembled) process, illustrated in figure 3, involves a sequence of steps to prepare and apply the cSEC onto a concrete surface for structural health monitoring. Initially, the adhesive copper tape is applied to the sensing area to establish an electrical connection for the Data Acquisition (DAQ) system, secured in place with paper tape as shown in figure 3(a). Following this, a copolymer CB solution is either brushed or sprayed onto the prepared area, serving dual functions as the electrode and the bonding agent, depicted

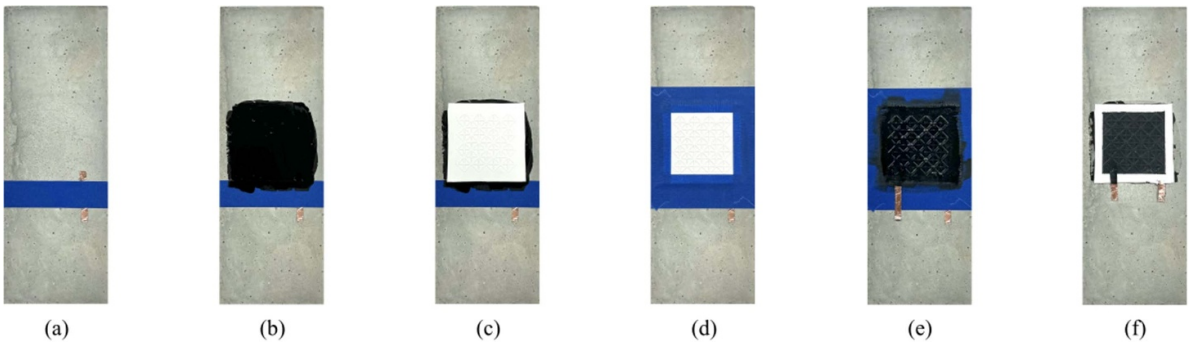


**Figure 3.** Step-by-step *in situ* assembly of the in cSEC on concrete showing (a) prepared concrete surface with a copper tape; (b) first electrode layer painted on the concrete surface; (c) placement of the dielectric layer on the electrode; (d) prepared surface of the dielectric layer for painting of the second electrode layer; (e) painted second electrode layer and second copper tape addition, and; (f) concrete sample showing an *in situ* assembled cSEC.

in figure 3(b). The dielectric layer is then immediately placed onto the wet CB solution, pressed to eliminate any air bubbles underneath, and left to dry for six hours to ensure a secure bond, as illustrated in figure 3(c). During this step, the cSEC is stretched approximately by 2% in planar directions to induce an initial strain that allows for compliant deformation with the concrete specimen. The surface of the dielectric is then prepared for application of the second electrode layer by applying paper tape as shown in figure 3(d). Next, a second layer of the copolymer CB solution is applied over the dielectric layer, and a second adhesive copper tape is attached to this top electrode, with the assembly then left to dry for twelve hours in a laboratory setting, as shown in figure 3(e). Upon completion of the drying process, the securing tapes are removed, resulting in a concrete sample equipped with a *in situ* assembled cSEC, ready for loading under a compression setup, as evidenced in figure 3(f).

The epoxied cSEC utilizes an off-the-shelf bi-component epoxy, such as JB Weld, for securing the cSEC detailed in the manufacturing section, to a pre-prepared surface. A thin, even layer of the epoxy adhesive is spread across the concrete surface, upon which the flat side of the cSEC is firmly placed, ensuring any air bubbles trapped under the sensor are meticulously removed. The setup is then left to cure in a controlled laboratory environment, with the drying time varying from a few minutes to several hours, depending on the specific epoxy formulation chosen. Preferred adhesives offer superior bonding strength, minimal shrinkage upon curing, and robust resistance to environmental factors, ensuring the durability and reliability of the sensor installation for long-term monitoring applications.

### 3.2. Cantilever aluminum plate test

The sensing performance of the *in situ* assembled cSEC, focusing on its sensitivity, signal linearity, and resolution, was evaluated using quasi-static and free vibration tests on a cantilever plate. The experimental setup, illustrated in figure 4(a), featured a homogeneous aluminum plate with dimensions of $406 \times 102 \times 3$ mm, one end of which was securely clamped between two grips of a dynamic testing system to form a cantilever configuration. A specific 76 mm by 76 mm area, positioned 90 mm from the free end of the plate, was designated as the sensing area. Here, the cSEC was applied using the *in situ* assembled method and allowed to cure for 12 h to ensure optimal adhesion. To mitigate potential noise interference stemming from the conductive base material used in the setup, a non-conductive primer was applied to the sensing area before applying the copolymer CB solution. Additionally, to provide a benchmark for the results, a foil-type resistive strain gauge (RSG) (C4A-06-235SL-350-39P by Micro-Measurements, with a nominal resistance of 350 Ω and a gauge length of 10 mm) was affixed to the opposite side of the plate at the exact location using an M-bond 200 adhesive kit, as depicted in the inset of figure 4(a).

Experiments consisted of subjecting the plate to a quasi-static load and free vibrations. In the quasi-static test, manual displacements were applied to the free end of the cantilever plate, both upwards and downwards, to induce tensile and compressive bending strains. For the free vibration test, the plate's free end was bent downwards approximately 70 mm from the grip position and then released, a process illustrated in the schematic of figure 4(a), to initiate free vibrations.

Data collection from the *in situ* assembled cSECs was executed using a BK Precision 891 LCR meter, referred to as the cSEC DAQ system in figure 4(b), with a sampling rate set at 45 samples per second ($\mathrm{S\,s^{-1}}$). Coaxial cables were utilized to connect the cSEC's copper tapes to the DAQ systems to ensure the integrity of the data by reducing parasitic noise. Additionally, precautions were taken to secure the cables and prevent any interference that might arise from their self-weight and movement during the testing process. For the foil type RSG, a 24-bit, 350-Ω, 3/4-bridge analog input module from National Instruments (NI-9236) was employed, capturing data at a sampling rate of 1000 $\mathrm{S\,s^{-1}}$. No signal filtering was applied to maintain the raw data integrity, and both DAQ systems operated concurrently within a LabVIEW programming environment, ensuring synchronous data acquisition and

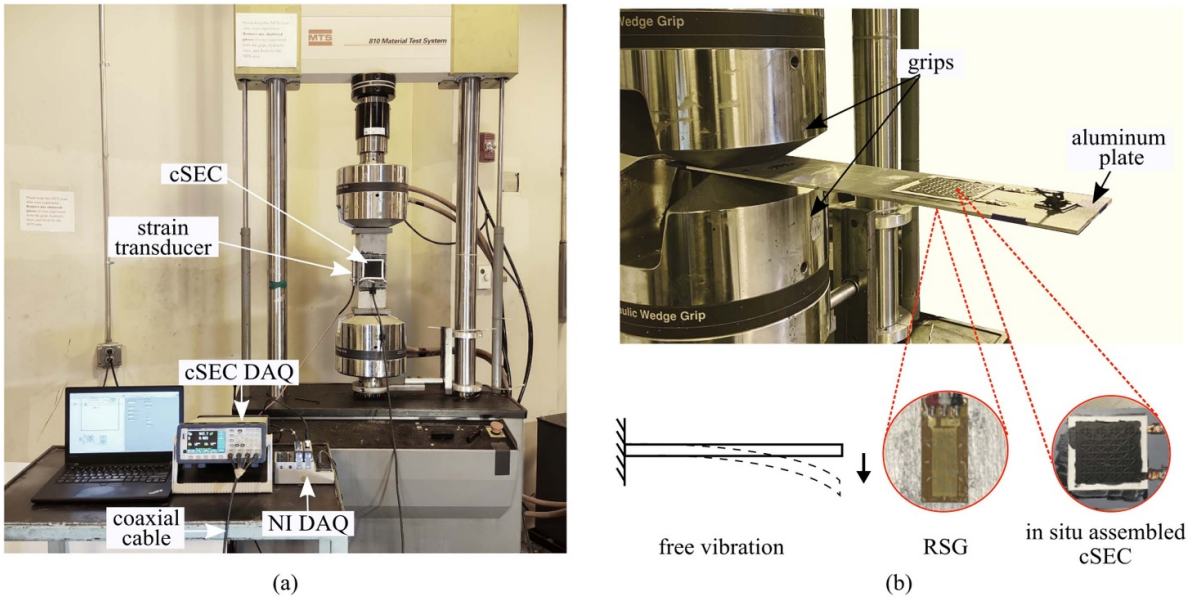


**Figure 4.** Experimental setup where (a) shows the setup for the dynamic compression test of concrete samples using material test system (MTS) alongside the data acquisition system; and (b) the cantilever plate constructed for quasi-static test and free vibration test.

facilitating a comprehensive analysis of the sensor's performance under quasi-static and dynamic loading conditions.

### *3.3. Concrete compression test*

Evaluating the *in situ* assembled cSEC affixed to unreinforced concrete specimens involved a series of compressive tests. These tests were performed using a closed-loop servo-hydraulic testing machine, specifically the MTS Model No. 609.25A-01, equipped to handle loads up to 250 kN, as depicted in figure 4(b). The concrete samples prepared for these tests conform to a specified mix design to ensure consistency and reliability in the results. This design included using a concrete mix with a compressive strength of 27 MPa (4000 psi), incorporating 3.5 liters of water for every 36.3 kg (80 pounds) of the mix, with an approximate density of 2014 kg $m^{-3}$ (125.73 lb $ft^{-3}$). The specimens were cured in a laboratory environment for at least seven days before testing to have strength for compression tests.

Two different sets of investigations were carried out on the concrete specimens. First, to understand the performance of the cSEC under various stress distributions and fracture behaviors on concrete, the concrete samples need to be of different sizes; hence, three unreinforced concrete sections with the size of 305 × 76 × 76 mm, 305 × 76 × 64 mm and 305 × 76 × 51 mm were prepared for this test. The size of the concrete samples is intrinsically linked to the distribution of stress and the nature of fracture behaviors. Larger concrete specimens tend to develop more complex stress fields due to the increased likelihood of inhomogeneities and varied internal stress paths. These differences can result in more intricate crack initiation and propagation patterns, which can be critical in evaluating the strain-sensing capabilities of the cSEC. The performance of the cSEC may vary across different sample sizes, making it essential to test a range of concrete sizes to fully understand the sensor's effectiveness in monitoring structural health under real-world conditions.

Two cSECs (*in situ* assembled and epoxied cSEC) were adhered to the sensing area on each concrete specimen's front and back surface by following the *in situ* assembled and epoxy bonding processes already illustrated. This dual-application approach allowed for a comparative analysis of the sensors' performance under identical testing conditions. Figure 5(a) presents the schematic of sensor positions on the concrete samples. A strain transducer (ST350 350-Ω strain transducer by BDI) was installed on the side surface to benchmark results, as shown in figures 5(b) and (c). The dimension of the three concrete samples used is shown in figure 5(d). The thickness of the dielectric layer painted on each concrete sample is the same at approximately 0.45 mm for each one, and epoxied cSEC of an approximate thickness of 0.30 mm was used alongside the *in situ* assembled cSEC. This consistency in cSEC thickness was critical for ensuring the reliability of the comparative analysis between the different bonding methods and concrete sample sizes.

Before the test, the concrete sample was pre-loaded to −35 kN to prevent signal drift caused by electrical interference with the dynamic testing machine and the initial settling of the concrete specimen under compression. Then, tests were started from a compressed state of −35 kN and performed by independently subjecting each cSEC-concrete specimen to a 0.05 Hz harmonic excitation in a fixed-compression mode between −25 kN and −35 kN for five cycles. cSEC data were collected using the same setup as the cantilever plate test, and the data measured by the strain transducer was recorded using the analog input module National Instruments NI-9237 at a

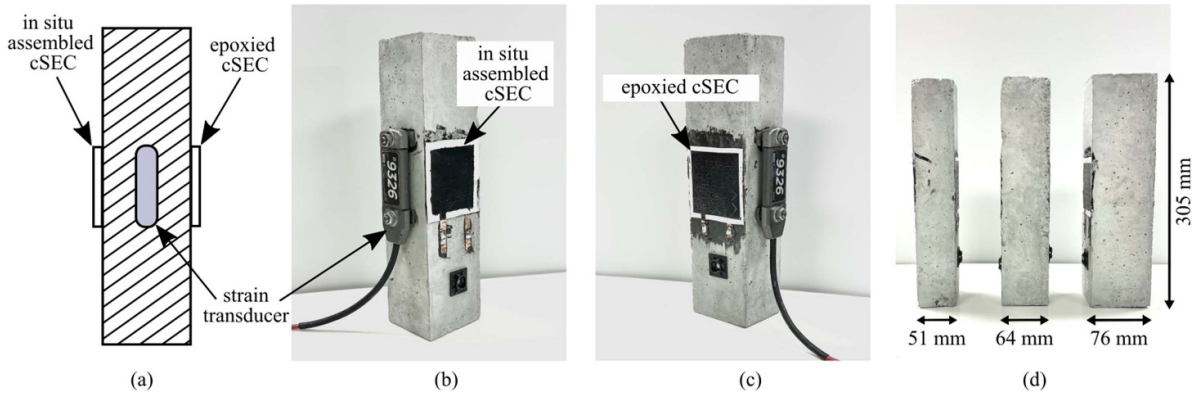


**Figure 5.** Concrete sample used for testing cSEC performance under various stress distributions and fracture behaviors, showing the, (a) schematic of the concrete sample showing the position of the cSECs and reference strain transducer; (b) concrete sample with cSEC attached using CB solution; (c) cSEC attached using an off-the-shelf bicomponent epoxy (JB Weld), and; (d) three concrete specimen with the thicknesses of 51, 64, and 76 mm.

sampling frequency of 1600 S $s^{-1}$. All compression tests were conducted in the laboratory under a constant temperature condition and were repeated at least three times for each specimen. A gauge factor of 1.7 is used for both *in situ* assembled and epoxied cSEC, facilitating a direct comparison between the performance characteristics of the two sensor types under identical testing conditions.

Preceding studies determined that the thickness of varying sensor layers influences structure/sensor capacitive coupling [28]. To further investigate this, various cSECs with different dielectric layer thicknesses were crafted and subjected to compression tests on a concrete specimen. cSECs with dielectric layer thicknesses of 0.23, 0.37, 0.40, 0.46, and 0.56 mm were tested for the *in situ* assembled application method. For the epoxy bonding method, the cSECs' thicknesses were 0.28, 0.36, 0.41, 0.48, and 0.56 mm to mirror those of the *in situ* assembled approach. These tests were carried out on a larger concrete sample with dimensions of 305 × 102 × 102 mm to ensure uniform testing conditions across all cSEC thickness variations, with the sensor thickness being the sole variable. The experimental setup and procedure are the same as the previous tests, albeit with an adjustment in the applied load to accommodate the larger size of the concrete specimen. Consequently, the load range was set between −22.5 kN and −45 kN, a modification intended to generate a clear and measurable signal from the sensors across the different thicknesses being evaluated. This comprehensive approach aims to pinpoint the optimal sensor thickness that maximizes the accuracy and reliability of strain measurements.

### *3.4. Peel test*

The adhesion strength of *in situ* assembled and epoxied cSEC on concrete and metal (specifically, aluminum) surfaces was assessed using a peel test according to the ASTM D903 at 180 degree peel angle. This experiment was designed to evaluate the bond durability of cSECs, each with a uniform thickness of 0.56 mm when adhered to rough and smooth concrete surfaces and abraded and smooth metal surfaces. This evaluation encompassed eight distinct bonding scenarios, utilizing the previously described *in situ* assembling and epoxy bonding methods.

The experimental setup for the peel test, as depicted in figure 6(a), involved positioning the cSEC-concrete specimen on a load frame, MTS Exceed E43 electromechanical load frame with a maximum loading capacity of 50 kN at a 45-degree angle. The concrete specimen was secured using a test piece support to ensure stability during the test, and a peel clearance was created at one corner edge of the cSEC. This clearance allowed for the attachment of the cSEC to a non-elastic tape, which was then held by the MTS grip, as illustrated in figure 6(c). A similar arrangement was employed for the aluminum plate setup, showcased in figure 6(d).

The peel test procedure commenced with the machine set to a zero-load condition, followed by a gradual increase in load at a steady linear rate of 60 mm $min^{-1}$. This process continued until the cSEC was peeled off to the halfway point from either the concrete or aluminum surface, as demonstrated in figure 6(d). Data on the loading force and displacement were collected at a sampling rate of 10 S $s^{-1}$ during this procedure. A visual inspection of both the cSEC and the substrate surfaces was conducted following the mechanical testing. This examination aimed to identify residual adhesive material and assess the failure modes incurred during peeling.

## 4. Results and analysis

This section presents and discusses the experimental results. First, the electromechanical behavior of a single *in situ* assembled cSEC is assessed. Second, the sensing performance

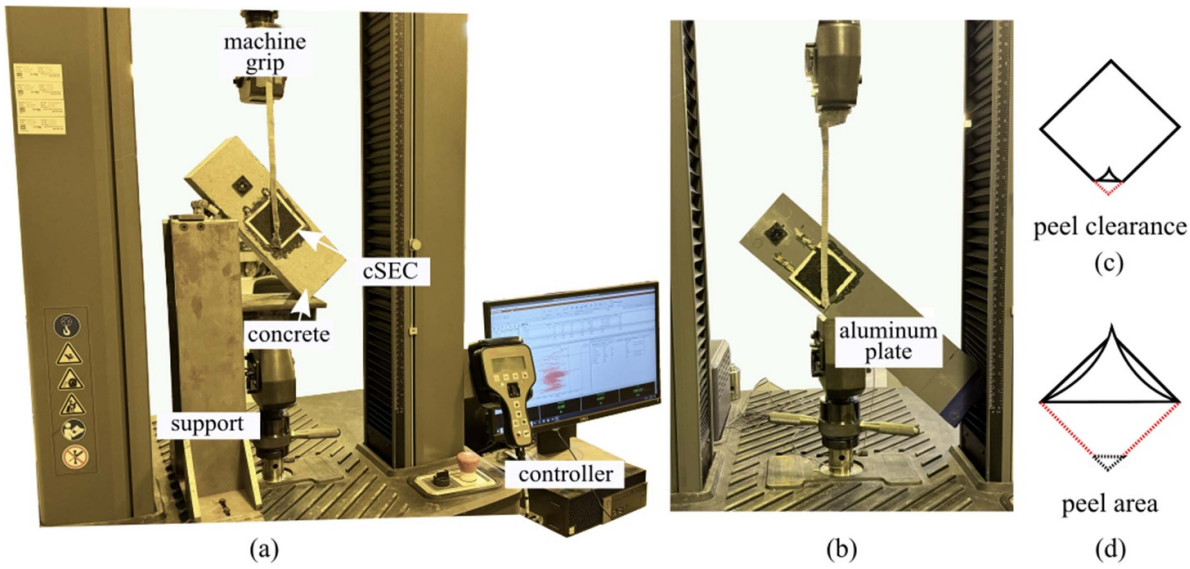


**Figure 6.** Experimental setup of the peel test showing; (a) concrete, (b) aluminum plate, (c) schematic of the peel clearance on the cSEC for adequate grip before peeling starts, and; (d) peel area after peeling test.

of the *in situ* assembled cSEC on concrete is compared against that of epoxied cSEC. Third, the dielectric layer thickness effect for *in situ* assembled cSEC and epoxied cSEC was also assessed. Lastly, the adhesion strength of *in situ* assembled and epoxied cSECs were reported.

### *4.1. Electro-mechanical behavior*

In the detailed examination of the sensing performance of *in situ* assembled cSEC, data from a quasi-static test conducted on a cantilever plate is analyzed. Figure 7(a) showcases a time series plot of the raw data capturing the relative change in capacitance, denoted as $\Delta C/C_0(\%)$, of the *in situ* assembled cSEC compared against the strain measurements obtained from a RSG, revealing a notable correlation between the two datasets. The precision of this correlation is quantitatively supported by a root mean square error (RMSE) of 0.21, indicating a strong agreement between the *in situ* assembled cSEC's readings and the established strain measurements from the RSG.

Further analysis is provided in figure 7(b), which plots the relative change in capacitance ($\Delta C/C_0(\%)$) against the applied strain, derived from the data showcased in figure 7(a). This plot also includes a linear fit, represented by a red solid line, obtained through least squares regression, illustrating the sensor's response to varying strain levels. Accompanying this linear fit is a 95% confidence interval, depicted by dotted-dashed blue lines, underscoring the statistical reliability of the linear relationship established. The *in situ* assembled cSEC exhibits a high degree of linearity within the examined strain range, extending from $-593$ to 394 $\mu\varepsilon$. This is further evidenced by an $R^2$ value of 0.986, which signifies an excellent fit between the observed data and the linear model. A high resolution in strain accuracy of 45 $\mu\varepsilon$, underscores the *in situ* assembled cSEC's capability to deliver precise and reliable strain measurements.

Figure 7(c) offers an insightful view into the performance of the *in situ* assembled cSEC alongside RSG measurements during a free vibration test. The test initiated vibrations within an approximate strain range of $\pm$ 300 $\mu\varepsilon$, gradually diminishing to $\pm$50 $\mu\varepsilon$ over approximately 1.7 s. This dynamic test scenario allowed the *in situ* assembled cSEC's proficiency in accurately mirroring the vibration profile to be observed, demonstrating its capability to follow the bending strain the RSG recorded closely. Further analysis is provided in figure 7(d), where a zoomed-in segment of the free vibration test reveals a minor temporal discrepancy in the sensor's signal-a lag of about 0.1 s. This delay is thought to result from slippage occurring at the bonding interface or potentially due to the differing response times inherent to the data acquisition systems utilized for the cSEC and RSG.

### *4.2. Concrete strain sensing*

Figure 8(a) shows the loading protocol for the analysis presented in figures 8(b)–(g) which offers a detailed comparison of strain data obtained from concrete samples of varying thicknesses-51, 64, and 76 mm-during the compression tests. This comparison pits the data measured by a strain transducer, serving as the reference, against the strain recorded by both *in situ* assembled cSEC and epoxied cSEC. The objective is to assess how the cSEC performs under different stress distributions and fracture behaviors characteristic of concrete samples of different thicknesses. The strain displayed by the cSEC was obtained using equation (6) with a gauge factor $\lambda$ of 1.7 for both *in situ* assembled and epoxied cSECs.

The findings reveal a closer alignment of the strain measurements from the *in situ* assembled cSEC with those from the strain transducer. In contrast, the epoxied cSEC tended to register higher strain values across all thicknesses of concrete specimens. This discrepancy aligns with observations reported

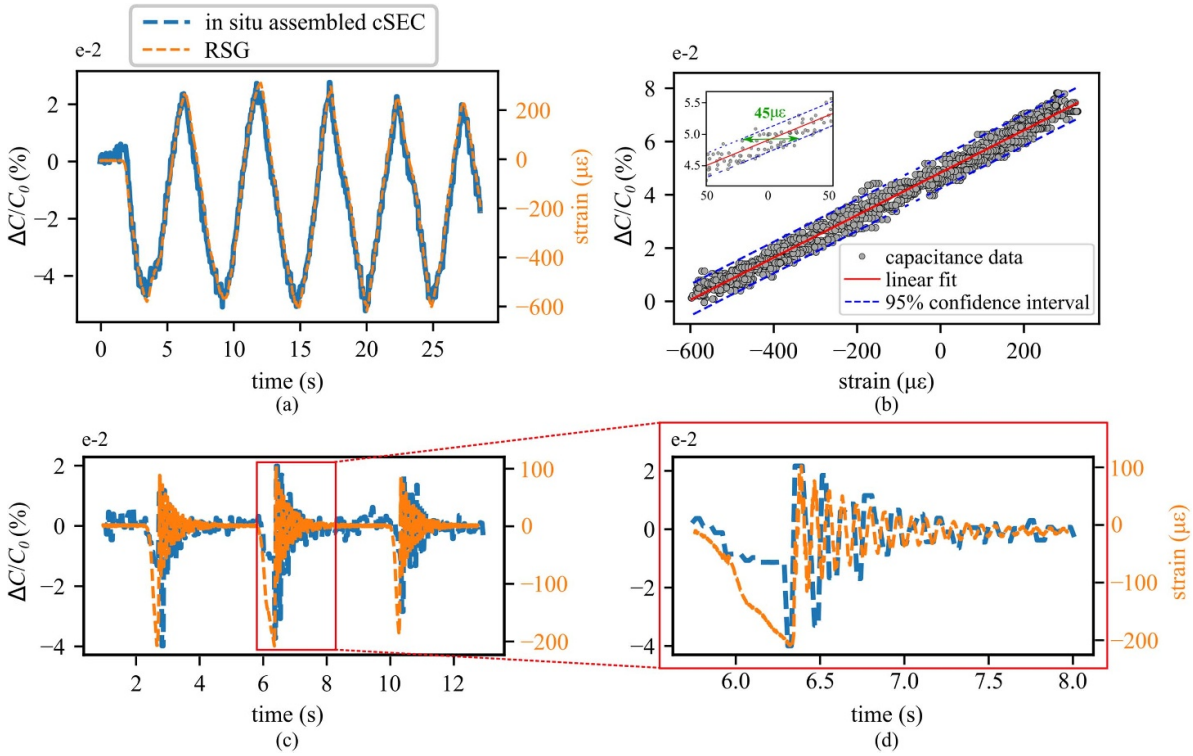


**Figure 7.** Electromechanical behavior of the SEC, showing: (a) time series plot from bending test; (b) results from a single *in situ* assembled cSEC, showing the relative change in capacitance $\Delta C/C_0(\%)$ versus applied strain measured from the RSG; (c) comparison of free vibration results from the *in situ* assembled cSEC and RSG; and (d) exploded free vibration plot from 5.5 s to 8 s.

in previous research [28] and can be attributed to the differences in the thickness of the cSEC employed in each adhesion method.

Further, figure 8(g) juxtaposes the peak strain amplitudes measured by the *in situ* assembled cSEC, epoxied cSEC, and the strain transducer across the various concrete thicknesses. Subsequent analysis, as shown in figure 8(h), quantifies the percentage difference in strain measurements relative to the strain transducer. This analysis indicates that the error margin in strain measurements decreases with increased concrete sample thickness. Notably, the *in situ* assembled cSEC consistently yielded strain measurements that were more accurate and closely matched the reference strain transducer, as compared to the epoxied cSEC.

Investigations on how the cSEC thickness influences their ability to accurately sense strain involved a systematic study across concrete samples with uniform dimensions (305 × 102 × 102 mm). This study meticulously documented in figures 9(a)–(j), compared the strain sensing results from *in situ* assembled cSEC (figures 9(a)–(e)) and epoxied cSEC (figures 9(f)–(j)), with sensor thicknesses ranging from 0.23 to 0.56 mm. It is important to note that the thickness values referenced herein pertain specifically to the thickness of the non-corrugated dielectric layer area of the cSEC rather than the overall sensor thickness. Variations in thickness across the different samples are largely due to the manual nature of the sensor fabrication process.

The analysis revealed a distinct pattern in strain measurement accuracy relative to the sensor thickness. Initially, there was a trend of overestimation in strain readings with thinner sensors (0.23 mm), which gradually transitioned to underestimation as sensor thickness increased to 0.56 mm. A notable observation was that *in situ* assembled and epoxied cSECs exhibited the closest match to the reference strain transducer data when the sensor thickness was around 0.40 mm. However, the correlation with the reference data weakened beyond this thickness, likely due to material compatibility issues that hinder effective strain transmission in thicker cSECs.

For a thinner sensor, the cSEC readings may include not only the actual strain but also other irrelevant variations that distort the true measurement. Conversely, the 0.56 mm thick sensor (figures 9(e) and (j)) shows reduced sensitivity to mechanical strain, as evidenced by the dampened strain signal, attributable to absorption of the strain energy caused by the thicker dielectric layer. This study underscores the critical role of sensor thickness in achieving accurate strain measurements, highlighting a sweet spot around 0.40 mm for *in situ* assemble cSEC and 0.41 mm for epoxied cSEC as they effectively correlated with actual mechanical strains, devoid of the distortions or dampening effects observed with thinner or thicker sensors, respectively.

Figure 10(a) visually represents the average peak strain amplitudes recorded by *in situ* assembled and epoxied cSECs during dynamic excitation tests. These tests span a range of sensor thicknesses, as detailed in figures 9(a)–(j). This graphical analysis reveals a trend where, with increasing thickness, the peak strain amplitudes measured by *in situ* assembled cSECs progressively align more closely with those recorded

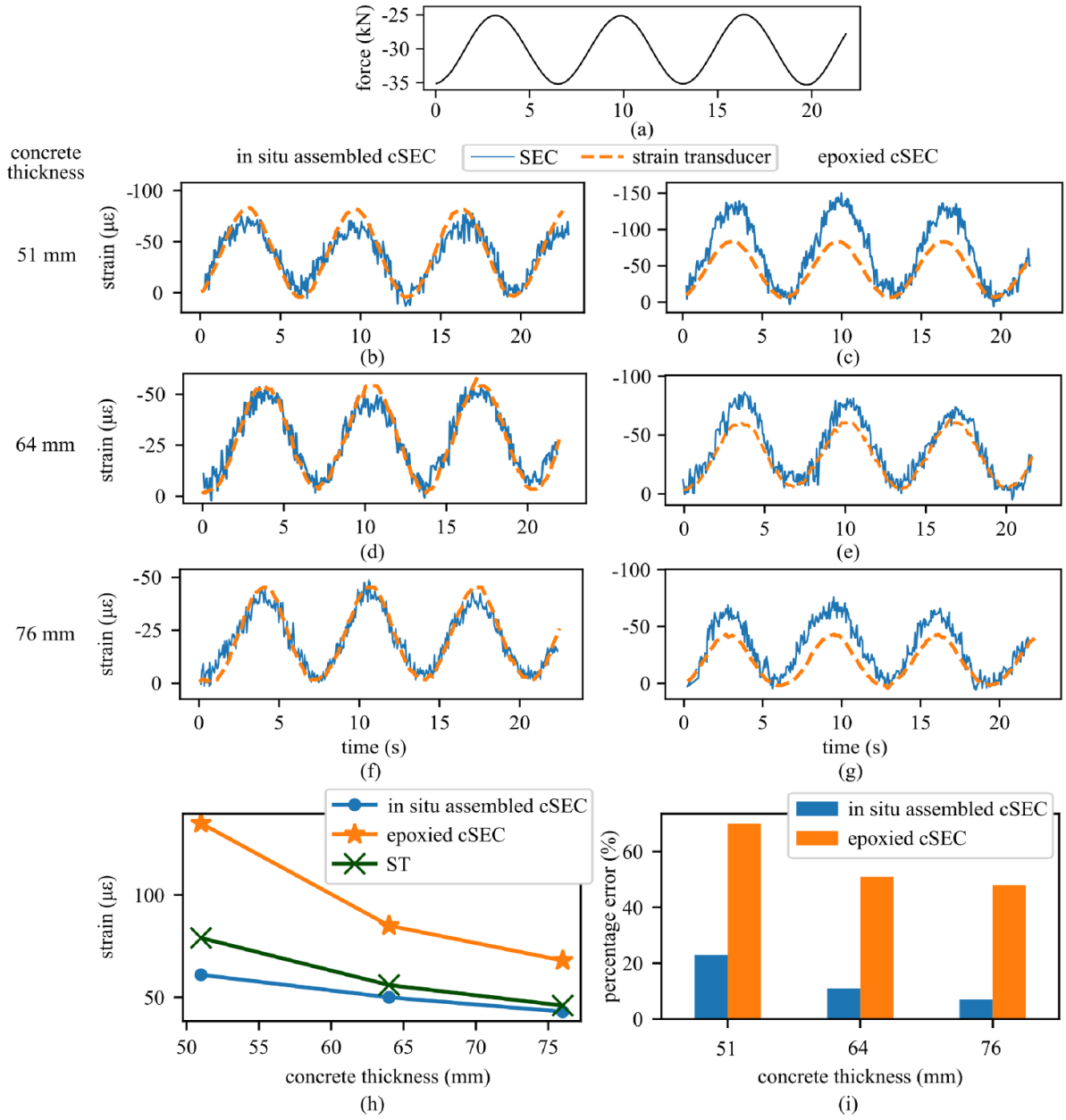


**Figure 8.** Strain data of *in situ* assembled cSEC and epoxied cSEC measured on concrete samples, showing: (a) concrete loading protocol, (b) and (c) 51 mm concrete thickness, (d) and (e) 64 mm concrete thickness, and (f) and (g) 76 mm concrete thickness; (h) comparison of strain measured from *in situ* assembled cSEC, epoxied cSEC and reference strain traducer on concrete samples with different thickness; (i) barplot of percentage error in strain of *in situ* assembled cSEC and epoxied cSEC computed in respect to the strain transducer.

by the reference strain gauge. Notably, optimal strain matching for *in situ* assembled cSECs occurs within the thickness range of 0.40–0.46 mm, while for epoxied cSECs, the ideal range is between 0.36 mm and 0.41 mm. To quantitatively assess the signal quality and evaluate the efficacy of *in situ* assembled and epoxied cSEC, two metrics were utilized: the decibel signal-to-noise ratio ($\mathrm{SNR_{dB}}$) and the mean absolute error (MAE).

$$\mathrm{SNR_{db}} = 10 \cdot \log_{10}\left(\frac{P_{\mathrm{signal}}}{P_{\mathrm{noise}}}\right) \tag{7}$$

$$\mathbf{MAE} = \frac{\sum_{i=1}^{z} |x_{\mathrm{true}_i} - x_{\mathrm{est}_i}|}{z} \tag{8}$$

where $P_{\mathrm{signal}}$ and $P_{\mathrm{noise}}$ in equation (7) are the time series data from the strain transducer and the cSEC, respectively. Analogously for $x_{\mathrm{true}_i}$ and $x_{\mathrm{est}_i}$ in equation (8), and $z$ is the the total number of samples collected.

Figure 10(b) elucidates the relationship between the signal-to-noise ratio (SNR) and the mean absolute error (MAE) in relation to the thickness of cSECs applied using *in situ* assembled and epoxied cSECs. This analysis reveals a critical point in sensor performance: as the thickness of the

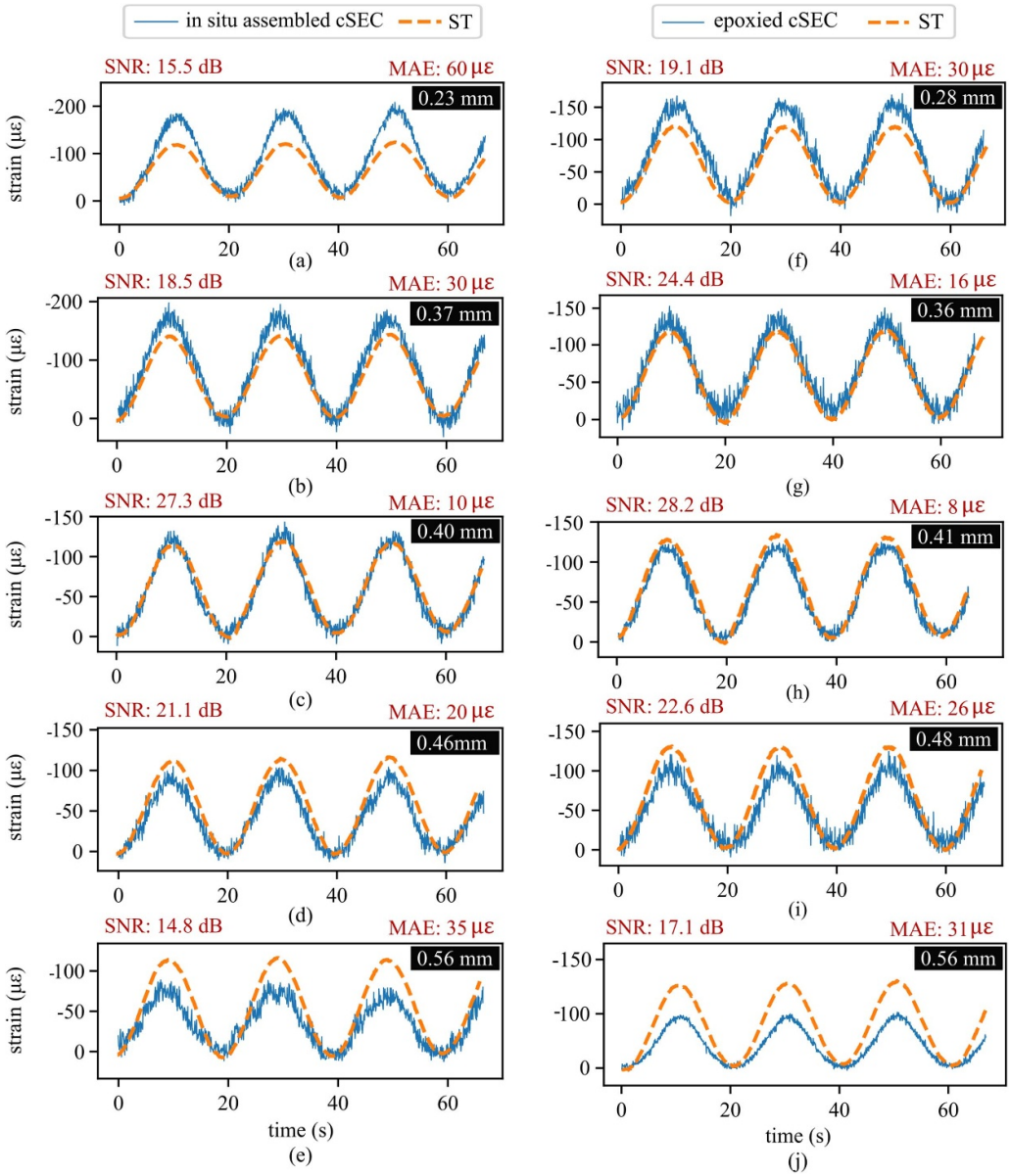


**Figure 9.** Time series of strain data on concrete for using *in situ* assembled cSEC of thicknesses of: (a) 0.23, (b) 0.37, (c) 0.40, (d) 0.46, and (d) 0.56 mm; and using epoxied cSEC of thickness of: (f) 0.28, (g) 0.36, (h) 0.41, (i) 0.48, and (j) 0.56 mm.

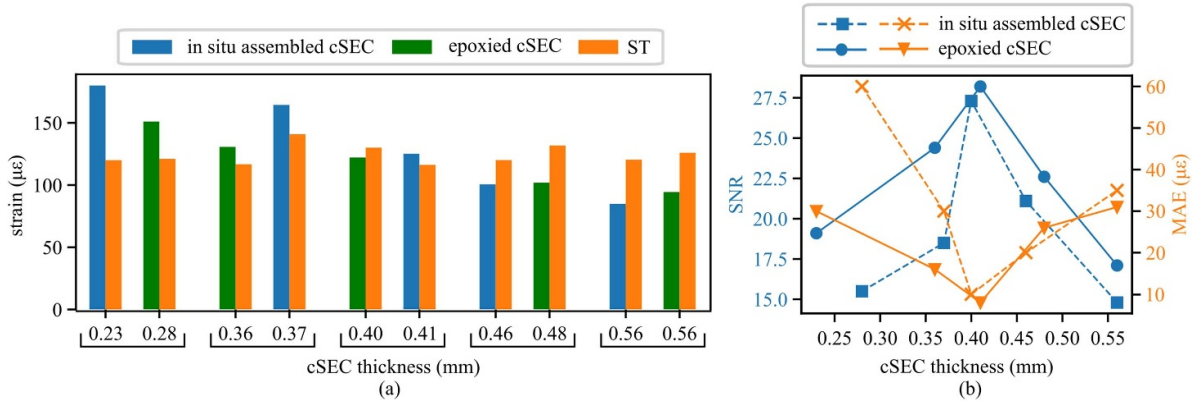


**Figure 10.** Metrics for evaluating the signal quality of the cSEC, showing (a) the barplot of *in situ* assembled and epoxied cSEC strain against the reference strain transducer, and; (b) MAE and SNR (dB) over different cSEC thicknesses.

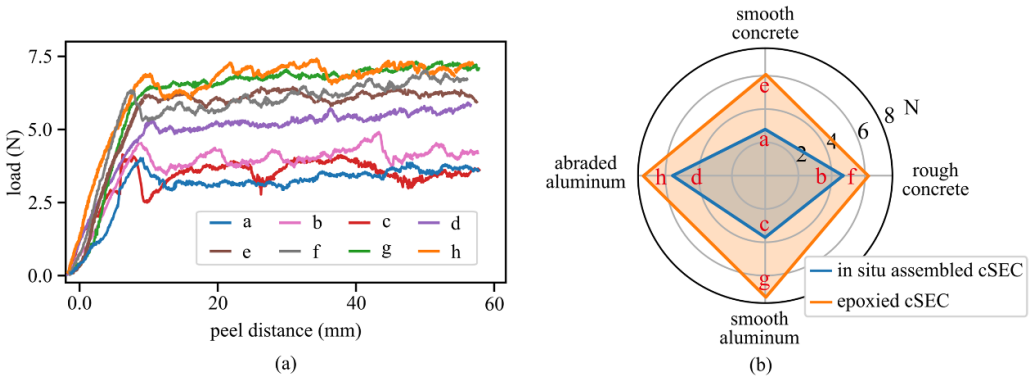


**Figure 11.** Adhesion strength test on *in situ* assembled and epoxied cSECs, showing: (a) the applied loads as a function of peel distance under different bonding case; and (b) a spider plot that compares the adhesion strength of *in situ* assembled and epoxied cSECs on adhered surface.

cSEC increases, the SNR improves, reaching a peak at around 0.40 mm for both bonding methods before it begins to decline. Conversely, the MAE demonstrates an inverse relationship, decreasing as the thickness approaches 0.40 mm and then increasing as the thickness further escalates. The optimal performance, characterized by a high SNR and a low MAE, is thus achieved with a cSEC thickness of approximately 0.40 mm under both bonding approaches. Specifically, SNR values peak at 27.3 dB for *in situ* assembled and 28.2 dB for epoxied cSEC, while MAE values are minimized to 10 $\mu\varepsilon$ for *in situ* assembled cSEC and 8 $\mu\varepsilon$ for epoxied cSEC. The implications of these findings suggest that an approximately 0.40 mm thick cSECs offers a balanced trade-off between sensitivity and accuracy, making it an ideal choice for future applications in monitoring the structural integrity of concrete structures.

### 4.3. Adhesion strength

Figure 11(a) provides a detailed graphical representation of the peel distance versus applied load for a series of test samples, identified as 'a' through 'h.' These samples encompass a range of variables, including different surface finishes (either smooth or rough), substrate materials (either concrete or aluminum), and the adhesion methods employed (*in situ* assembled with CB and epoxy bonding), as further elaborated in figure 11(b). The depicted curves illustrate a consistent pattern across all samples, where the applied load increases in tandem with the peel distance up to a critical point of approximately 10 mm. Beyond this threshold, the load required for further peeling plateaus maintains a near-constant level up to around 60 mm, corresponding to the halfway mark of the sensor being peeled off from the surface. This initial rise in load reflects the cumulative effect of adhesive forces at play, which must be progressively overcome to initiate and continue the peeling process. The subsequent stabilization in the peeling force indicates a transition to a second failure mode, where the adhesion between the sensor and the adhered surface has been sufficiently disrupted, such that a larger load is not required for further separation.

Figure 11(b) is a spider plot that compares the adhesion strength of the *in situ* assembled and epoxied cSECs on concrete and aluminum surfaces tested from the peel test in figure 11(a). It can be seen that the epoxied cSEC (orange color) method has a stronger bonding by exhibiting a 32%–98% higher bonding strength than the *in situ* assembled cSEC (blue color). The bonding strength on the smooth aluminum surface provided by the epoxy bonding and CB painting are respectively 19% and 33% higher than that on the smooth concrete surface, attributable to the smoother and more uniform texture on metal surfaces that provide better intimate contact and molecular interaction between the epoxy layer and the metal. Similarly, bonding strength on the abraded aluminum surface provided by the epoxy bonding and CB painting are both about 19% higher than that on the rough concrete surface.

It can also be observed that the average peel-off force of epoxied cSEC on the concrete and aluminum surfaces was nearly constant at 7.42 and 6.21 N, respectively, regardless of the surface roughness. While the adhesion strength of the *in situ* assembled cSEC varied more significantly depending on the surface roughness, the average peel-off force on the rough concrete and mechanically abraded metal are respectively 50%–68% higher than those on their smooth surfaces, likely attributable to the enhanced mechanical interlocking between the sensor and bonding layer.

Figures 12(a) and (b) provide visual evidence of the failure modes encountered by the cSECs following the peel tests, highlighting the differences in adhesive behavior between *in situ* assembled with CB and epoxy bonding methods. The *in situ* assembled cSEC exhibits uneven adhesive residue distribution across the sensor surface, indicating that the adhesive forces were not consistently applied throughout the bonding area. This unevenness suggests potential areas of weak adhesion, which could compromise the overall integrity and performance of the sensor under detrimental in-service environmental conditions. In contrast, the epoxied cSEC shows a more uniform layer of adhesive residue, pointing towards a more consistent and stronger bond throughout the contact area between the sensor and the substrate. This uniformity aligns

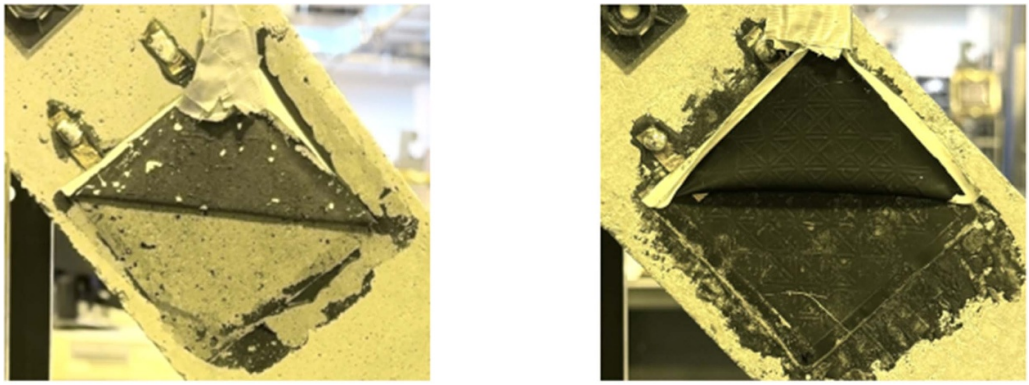


**Figure 12.** Adhesive failure mode on (a) *in situ* assembled cSEC; and (b) epoxied cSEC.

with the experimental findings that indicate a higher bonding strength in the epoxied cSEC compared to *in situ* assembled cSEC. The visual inspection corroborates the quantitative data, reinforcing that epoxy resin provides a more robust and reliable bond.

Despite the stronger bond achieved with epoxy resin, it is noteworthy that the *in situ* assembled cSEC offers an advantage in terms of strain measurement accuracy on concrete surfaces and the increased simplicity of having a sensor attached to a structure without the need for an extra bonding layer. Methodologies to improve the CB solution bonding strength are left for further research. While the proposed cSEC technology demonstrates promise for SHM, challenges such as ensuring proper surface preparation on rough concrete surfaces may arise in real-world applications, which could affect sensor adhesion and performance. Also, mitigating environmental factors such as temperature fluctuations and humidity, could impact sensor durability. The sensor's flexibility offers it as a unique option for complex geometries with minimal surface preparation required on most monitored structures before adhering the sensor.

## 5. Conclusion

This paper presents a detailed investigation into the *in situ* assembly of corrugated Soft Elastomeric Capacitors for the purpose of structural health monitoring on concrete structures. The study successfully demonstrates the viability of using a Carbon Black solution as both an adhesive and an electrode, providing a simpler and more efficient alternative to traditional epoxy bonding methods.

The methodology included a quasi-static and free vibration test conducted on the aluminum cantilever plate to characterize the sensing properties of *in situ* assembled cSEC in terms of linearity, resolution, and strain-tracking capability. Compression tests were designed and conducted on concrete specimens with varied thicknesses, as well as using varying sensor thickness to evaluate the strain-sensing performance of cSEC. Strain data were compared to data from off-the-shelf strain transducers. Finally, a peel test was conducted to evaluate adhesion strength of the technique.

Results show that the *in situ* assembled cSEC exhibited good linearity with an $R^2$ value of 0.986 and a 45 $\pm\mu\varepsilon$ resolution. Optimal sensor thickness lies between 0.40 mm and 0.46 mm for strain sensing on concrete with high SNR of up to 27.3 dB and the low MAE of 10 $\mu\varepsilon$ for the *in situ* assembled cSEC. Although the epoxied cSEC demonstrated a higher bonding strength that exceeded the *in situ* assembled cSEC method by 32%, the *in situ* assembled cSEC method maintained effective strain transmission capabilities, with its adhesion strength improved on rougher surfaces.

Future research directions include enhancing the CB solution with stronger bonding agents to combat environmental degradation and ensure the longevity of the sensor's adhesion which is its potential limitation, marking a promising step forward in structural health monitoring. This study lays the groundwork for innovative sensor manufacturing practices that could streamline and improve the efficiency of monitoring concrete infrastructures.

## Data availability statement

All data that support the findings of this study are included within the article (and any supplementary files).

## Acknowledgments

The authors gratefully acknowledge the financial support of the Departments of Transportation of Iowa, Kansas, South Carolina, and North Carolina, through the Transportation Pooled Fund Study TPF-5(449).

## Conflict of interest

The authors declare no conflict of interests.

## ORCID iDs

Emmanuel Ogunniyi https://orcid.org/0000-0001-5456-5929
Han Liu https://orcid.org/0000-0003-3057-522X
Austin RJ Downey https://orcid.org/0000-0002-5524-2416
Simon Laflamme https://orcid.org/0000-0002-0601-9664
Jian Li https://orcid.org/0000-0003-3439-7539
Caroline Bennett https://orcid.org/0000-0002-2713-0011
William Collins https://orcid.org/0000-0002-2835-6389
Hongki Jo https://orcid.org/0000-0001-5056-1154
Paul Ziehl https://orcid.org/0000-0002-4783-9255

## References

[1] Farrar C R and Worden K 2007 *Phil. Trans. R. Soc.* A **365** 303–15
[2] Gharehbaghi V R, Noroozinejad Farsangi E, Noori M, Yang T Y, Li S, Nguyen A, Málaga-Chuquitaype C, Gardoni P and Mirjalili S 2022 *Arch. Comput. Methods Eng.* **29** 2209–35
[3] Lynch J P and Loh K J 2006 *Shock Vib. Dig.* **38** 91–130
[4] Zhu L, Fu Y, Chow R, Spencer J B F, Park J W and Mechitov K 2018 *Sensors* **18** 262
[5] Wang X, Jin Z, Liu J, Chen F, Feng P and Tang J 2021 *Constr. Build. Mater.* **266** 121018
[6] Divsholi B S and Yang Y 2014 *NDT&E Int.* **65** 28–34
[7] Chakraborty J, Katunin A, Klikowicz P and Salamak M 2019 *Sensors* **19** 3879
[8] Sieńko R, Zych M, Ł B and Howiacki T 2019 *Struct. Health Monit.* **18** 1510–26
[9] Silva K S, Silva F, Mahfoud T, Khelidj A, Brientin A, Azevedo A, Delgado J M and de Lima A G B 2021 *Sensors* **21** 4171
[10] Alwis L S, Bremer K and Roth B 2021 *Sensors* **21** 4948
[11] Gomasa R, Talakokula V, Jyosyula S K R and Bansal T 2023 *Constr. Build. Mater.* **405** 133179
[12] Cheilakou E, Tsopelas N, Anastasopoulos A, Kourousis D, Rychkov D, Gerhard R, Frankenstein B, Amditis A, Damigos Y and Bouklas C 2018 *Proc. Struct. Integrity* **10** 25–32
[13] Simon A, Courtois A, Clauzon T, Coustabeau E and Vinit S 2015 Long-term measurement of strain in concrete: durability and accuracy of embedded vibrating wire strain gauges *3rd Conf. on Smart Monitoring, Assessment and Rehabilitation of Civil Structures (SMAR)* pp 7–9
[14] Qiu Z, Wu J and Yuan S 2011 *Meas. Sci. Technol.* **22** 075205
[15] Mishra M, Lourenço P B and Ramana G V 2022 *J. Build. Eng.* **48** 103954
[16] Zhu H-H, Liu W, Wang T, Su J-W and Shi B 2022 *Sensors* **22** 7550
[17] Thiele M and Pirskawetz S 2022 *Materials* **15** 341
[18] Markov V, Kupiec S, Weldon J, Abejar J and Erwin D 2022 Laser doppler imaging vibrometer for real-time health monitoring of civil infrastructures *Proc. SPIE* **12047** pp 293–302
[19] Seo H 2021 *Tunn. Undergr. Space Technol.* **116** 104118
[20] Jung Y H, Park B, Kim J U and Kim T-I 2019 *Adv. Mater.* **31** 1803637
[21] Masciotta M G, Barontini A, Ramos L F, Amado-Mendes P and Lourenço P B 2019 *Int. J. Bio-Inspired Comput.* **14** 1–26
[22] Laflamme S, Saleem H S, Vasan B K, Geiger R L, Chen D, Kessler M R and Rajan K 2013 *IEEE/ASME Trans. Mechatronics* **18** 1647–54
[23] Rácz Z, Hackney E M and Wood D 2016 *Proc. Eng.* **168** 721–4
[24] Fassler A and Majidi C 2013 *Smart Mater. Struct.* **22** 055023
[25] Taher S A, Li J, Jeong J-H, Laflamme S, Jo H, Bennett C, Collins W N and Downey A R J 2022 *Sensors* **22** 5076
[26] Liu H, Laflamme S, Li J, Bennett C, Collins W, Downey A, Ziehl P and Jo H 2021 *Smart Mater. Struct.* **30** 105030
[27] Downey A, Pisello A L, Fortunati E, Fabiani C, Luzi F, Torre L, Ubertini F and Laflamme S 2019 *Sens. Actuators* A **293** 269–80
[28] Ogunniyi E, Vareen A, Downey A R J, Laflamme S, Li J, Bennett C, Collins W, Jo H, Henderson A and Ziehl P 2023 *Meas. Sci. Technol.* **34** 055113
[29] Ogunniyi E A, Liu H, Downey A R J, Laflamme S, Li J, Bennett C, Collins W, Jo H and Ziehl P 2023 Soft elastomeric capacitors with an extended polymer matrix for strain sensing on concrete *Proc. SPIE* **12486** 262–70
[30] Devaraj H, Schober R, Picard M, Teo M Y, Lo C Y, Gan W C and Aw K C 2019 *Meas. Sens.* **2** 100004
[31] Atalay O 2018 *Materials* **11** 768
[32] Wang L, Wang Y, Yang S, Tao X, Zi Y and Daoud W A 2022 *Nano Energy* **91** 106611
[33] Davis M J and McGregor A 2010 Assessing adhesive bond failures: mixed-mode bond failures explained *ISASI Australian Safety Seminar, Canberra* pp 4–6
[34] Liu H, Laflamme S and Kollosche M 2023 *Sensors* **23** 6146
[35] D903-98R17 A D 2017 ASTM International West Conshohocken, PA